The Estimated Climate Impact of the Hunga Tonga-Hunga Ha'apai Eruption Plume

M. R. Schoeberl & Y. Wang, Science and Technology Corporation, Columbia, MD, USA

R. Ueyama, NASA Ames Research Center, Moffett Field, CA, USA

A. Dessler, Texas A&M University, College Station, TX, USA

G. Taha, Morgan State University, Baltimore, MD, USA

W. Yu, Hampton University, Hampton, VA, USA

Corresponding Author: Mark Schoeberl (mark.schoeberl@mac.com)

Submitted to GRL 5/20/2023

Key Points

- Following the Jan. 15, 2020 Hunga-Tonga eruption, both aerosols and water vapor increased in the stratosphere.
- The stratospheric water vapor increases the net downward radiative flux up to 0.3 W/m^2 and aerosols reduce the solar flux up to ~1.5 W/m^2
- The reduction in radiative forcing by the Hunga-Tonga eruption will very slightly cool the Southern Hemisphere.

Plain Language Summary

The Hunga Tonga-Hunga Ha'apai (HT) submarine volcanic eruption on January 15, 2022 produced aerosol and water vapor plumes in the stratosphere. These plumes have persisted mostly in the Southern Hemisphere throughout 2022. Enhanced tropospheric warming due to the added stratospheric water vapor is offset by the larger stratospheric aerosol attenuation of solar radiation. The change in the radiative flux could result in a very slight cooling in Southern Hemisphere surface temperatures.

Abstract

On Jan. 15, 2022, the Hunga Tonga-Hunga Ha'apai (HT) eruption injected SO_2 and water into the middle stratosphere. The SO_2 is rapidly converted to aerosols. The aerosol and water vapor anomalies have persisted in the Southern Hemisphere throughout 2022. The water vapor anomaly increases the net downward IR radiative flux whereas the aerosol layer reduces the direct solar forcing. The direct solar flux reduction is larger than the increased IR flux. Thus, the net tropospheric forcing will be negative. The changes in radiative forcing peak in July and August and diminish thereafter. Scaling to the observed cooling after Pinatubo, HT would cool the Southern Hemisphere's average surface temperatures by less than 0.038°C.

Index Terms

0340 Middle atmosphere dynamics

0341 Middle atmosphere: constituent transport and chemistry

0370 Volcanic effects

1. Introduction

The Hunga Tonga-Hunga Ha'apai (HT) (20.54°S, 175.38°W) erupted on Jan. 15, 2022, with a volcanic explosivity index of five, comparable to eruption of Krakatoa in 1883 (Carn et al., 2022, C22). As shown in Microwave Limb Sounder (MLS) measurements (Millán et al., 2022, hereafter M22) and balloon sondes measurements (Vomel et al. 2022), a significant amount of water vapor was injected into the tropical Southern Hemisphere (SH) mid-stratosphere. HT also injected about 0.5 Tg – 1.5 Tg of SO_2 (C22, Sellitto et al., 2023) which produced an aerosol layer that was detected by the Ozone Mapping and Profile Suite (OMPS) limb sounder (LP) (Taha et al., 2022). Although SO_2 injection was modest for an eruption of this size (C22; M22), the MLS estimated water injection was 146 Tg or ~10% of the total stratospheric water vapor prior to the eruption (M22). The water vapor and aerosol plumes from the HT eruption have persisted in the SH throughout 2022 (Schoeberl et al., 2023). The stratospheric water vapor anomaly led to a mid-stratospheric cooling of ~ 4° K in March-April (Schoeberl et al., 2022, hereafter S22) due to the increased outgoing IR radiation.

Historically, the SO_2 from large volcanic eruptions produces an abundance of aerosols that causes temporary decrease in tropospheric temperatures due to the reduction in solar radiative forcing (Yu and Huang, 2023; Aurby et al., 2021; Stenchikov, 2016; Hansen et al., 2002). Volcano-sourced sulfuric acid aerosols can persist for years and even self-loft (Khaykin et al., 2022). Stratospheric aerosols reduce the direct solar flux and changes in surface temperatures have been observed after large eruptions (Fujiwara et al., 2020, Crutzen, 2006).

Changes in stratospheric water vapor can also contribute to changes in climate forcing (Forster and Shine, 1999). Solomon et al. (2010) estimated that the tropical, lower stratospheric decrease of ~0.4 ppmv H_2O between 2000 and 2005 would reduce tropospheric forcing by ~0.098W/m^2. This forcing results from changes in the long-wave IR (LWIR) emission and short wave IR (SWIR) attenuation. Consistent with the Solomon et al. (2010) study, Dessler et al. (2013) determined the sensitivity of the of the climate system to tropical stratospheric water vapor and calculated a water vapor feedback parameter of 0.27 W/m^2/ppmv.

Models predict that stratospheric H_2O will increase as the climate warms. Basically, the tropical tropopause cold trap warms allowing more water vapor into the stratosphere, although this effect is somewhat mitigated by the strengthening Brewer-Dobson circulation (Xia et al., 2019). Banerjee et al. (2019) analyzing CMIP5 models computed the stratospheric water vapor component of the climate feedback to be 0.14 W/m^2/K for 4xCO_2. Li and Newman (2020) using the Goddard Earth Observing System Chemistry-Climate model computed a similar water vapor feedback value of 0.11 W/m^2/K. A much smaller response (0.02-0.03 W/m^2/K) was found by Huang et al. (2016, 2020). Note that these model studies are evaluating the long-term climate-system response where non-atmospheric systems (e.g. the ocean, cryosphere) have time to equilibrate. The short-term atmospheric response to sudden forcing changes may be larger because the system is out of equilibrium (Dessler and Zelinka, 2015).

Given the observed climate sensitivity to stratospheric water vapor (Dessler et al., 2013), it is logical to assume that HT might have a climate impact. Jenkins et al. (2022) used a parameterized climate-response model to investigate the impact of the HT water vapor plume.

They neglected the impact of aerosols and only considered the radiative forcing due to the water vapor. Jenkins et al. (2022) computed a 0.12 W/m^2 increase in tropospheric radiative forcing. M22 arrived at a similar number, 0.15 W/m^2. On the other hand, Sellitto et al. (2022) and Zhu et al. (2023) added the direct aerosol forcing and estimated that the plume would produce a peak forcing of -1 to -2 W/m^2. This exceeds the estimated H_2O IR forcing. Clearly, both the net warming due to the H_2O and cooling due to the aerosol layer need to be considered.

In this study we extend the computation of the radiative forcing by Zhu et al. (2022) and Sellitto et al. (2022) combining the H_2O and aerosol radiative forcing. We compute the downward flux change due to stratospheric water vapor using a radiative transfer model. Because of the complexity of computing the aerosol forcing, we take a different approach to estimate the reduction in solar flux. We first use OMPS-LP measurements of stratospheric aerosol extinction to compute the stratospheric aerosol optical depth (AOD). We then convert the AOD to changes in direct radiative forcing using a parameterization based on AOD estimates and direct forcing from previous volcanic eruptions. This approach is also used in climate assessment models (e.g. Hansen et al., 2002, hereafter H2002). To check our parameterization, we also use the aerosol direct radiative forcing parameterization in Yu and Huang (2023) (hereafter YH). YH provides climatology kernels that can be used to convert AOD to aerosol direct forcing under both clear and all sky (cloudy) conditions.

2. Data sets

We use Microwave Limb Sounder (MLS) V5 for temperature and H_2O measurements. The data quality for the HT anomaly is detailed in M22 and MLS data is described in Livesey et al. (2021). We restrict our constituent analysis to below 35 km, which is roughly the maximum height of the plume a few weeks after the eruption.

We use the aerosol extinction data from OMPS-LP, level-2 V2.1 . The V2.1 data (Taha et al.,2022) provides the most accurate OMPS-LP aerosol retrieval up to 36 km. Although the extinction measurements by OMPS-LP are generally consistent with those made by SAGE III/ISS, the OMPS-LP algorithm may overestimate the aerosol extinction below the aerosol peak (Bourassa et al., 2023). AOD is computed from OMPS-LP extinction at 600 nm by integrating the extinction from 36 km to the tropopause height included in the OMPS-LP files. The AOD is converted from 600 nm to 550 nm assuming an Ångstrom exponent of 1.0 which was derived from SAGE III/ISS HT observations (Taha et al.,2022). The daily MLS and OMPS data sets are averaged onto a 5°x10° latitude-longitude grid.

We show the SO_2 eruption data available from the NASA Multi-Satellite Volcanic Sulfur Dioxide L4 Long-Term Global Database produced as part of the NASA MEaSUREs project (Carn et al., 2022).

3. Analysis

In the sections below, we describe our approach to estimating the changes in tropospheric forcing due to HT aerosols and stratospheric water vapor.

3.1 Parameterization of the direct solar radiative forcing by aerosols

Figure 1a shows the variations in OMPS-LP AOD during 2022; both the maximum AOD and global average AOD are shown. The figure shows a rapid increase in maximum AOD following the eruption which is followed by a slower growth rate until mid-April. Anomalies and gaps in the late July and early August data are due to a spacecraft anomaly. Although the peak AOD reaches 0.05, the global average AOD only reaches ~0.02 because most of the aerosol stays within the SH (S22; Taha et al., 2022). Simulations by Zhu et al. (2022) show that SO_2 is converted to sulfate aerosols rapidly following the eruption – a process enhanced by the abundance of water vapor in the plume. After mid-April, dispersion of the aerosols combined with settling cause a slow decrease from the maximum AOD.

H2002 assumed that the aerosol driven change in the direct solar radiative forcing (ΔA) can be approximated by $\Delta A = -R\ AOD$, R=21. YH derived direct radiative forcing kernel maps from reanalysis to convert AOD to ΔA, but avoided large volcanic eruption periods. The YH global average clear sky conversion factor R is 29.4, and for all skies, R=15.7.

The stratospheric AOD changes associated with volcanic eruptions can be much larger than the observed AOD perturbations in the 2000-2022 period YH analyzed. We therefore have independently derived our own parameterization from volcanic analyses. Table 1 shows a list of major observed eruptions and one simulated eruption (Aubry et al., 2021) along with their estimated SO_2 emission, the maximum globally averaged AOD, and the maximum global direct forcing (ΔA W/m^2). Using these AOD values and our estimates, we can compute the HT direct forcing. We set the background stratospheric AOD is set to 0.012 which is an offset since we want to compute $\Delta A(volcanic\ only)$. Figure 1b shows the estimated change in solar flux, ΔA, vs AOD for the data in Table 1 with each volcano listed. We also show a linear fit and log_e(AOD) fit to volcanic AOD, H2002 parameterization, and both YH parameterizations. We find R = 19.5 for our linear fit, which is close to the H2002 value of 21. Figure 1b shows that the log_e fit better reproduces the estimated changes in ΔA compared to the linear fit. The log_e fit is

$$\Delta A = -(5.58 + 1.26 \log_e(AOD)) \text{ W/m}^2 \qquad (1)$$

Table 1 also shows that YH clear sky parameterization produces a result very close to the results using (1).

3.2 Radiative forcing changes due to Hunga-Tonga

3.2.1 Changes in direct solar forcing due to aerosols

For the maximum HT global average AOD value of 0.02, (1) gives a peak global decrease in solar flux (ΔA) of -0.64 W/m^2 (Fig. 1b, red dot; Table 1). Using the H2002 parameterization we estimate the change is -0.42 W/m^2. The YH parameterization gives -0.54 W/m^2 for clear skies and -0.29 W/m^2 for all skies. Zhu et al. (2022)'s estimate of -0.25 W/m^2 is slightly lower, because they averaged the forcing in February before the peak AOD in March-April and their simulated aerosol cloud is less extensive than that observed by OMPS-LP (their Fig. 3).

Figure 2a shows the surface area weighted zonal mean AOD and aerosol solar radiative forcing due to HT (Fig. 2b) from Eq. (1). Although Eq. (1) is derived using global averages, there is no reason to believe it would not be valid for local changes in solar flux because the approximation simply links stratospheric AOD directly to solar flux. As a check on this assumption, we also perform the calculation using YH kernel maps and these calculations are also shown in Fig. 2 (c, d). Our parameterization and YH clear sky are nearly identical, suggesting that YH can be extended to volcanic events the size of HT. Figure 2d shows that if clouds are included the direct solar decreases by about a factor of ~2. From hereafter we will use the YH parameterization.

The evolution of the direct solar forcing follows the spatial changes in AOD as might be expected, and the decrease in solar forcing is mostly confined to the SH. Our estimates of solar flux changes are in good agreement with estimates by Sellitto et al. (2022). Figs. 2 also shows a southward shift in the aerosol distributions near day 150 (May 30), and this is reflected in changes in forcing. Sellitto et al. (2023) also shows this southward shift (their Fig. 1b)

3.2.2 Changes in IR radiative forcing due to water vapor

HT produced an enhanced, mostly SH, stratospheric water vapor layer that mostly extends between 22 and 30 km. This layer generates additional downward LWIR fluxand also slightly reduces the solar flux due to water vapor radiative absorption in the SWIR bands. We use the radiative transfer model (RTM) described by Mlawer et al. (1997) to compute the downward radiative flux changes produced by this layer using MLS observed trace gases and temperatures.

To quantify the flux changes, we first compute a daily climatology of MLS temperature and trace gases using 2016-2021 data. We calculate the difference between the 2022 downward tropopause fluxes and the downward fluxes computed using the climatology. We have not applied any adjustment to temperature (e.g. fixed dynamical heating) due to water vapor cooling in the radiative forcing calculations, as was done in previous work (Solomon et al., 2010; Dessler et al.,2013). Solomon et al. (2010) shows that the instantaneous forcing and adjusted forcing are very similar above 22 km. Since HT's water vapor was mostly injected above that altitude, the adjustment is unimportant. Jenkins et al. (2023) also did not perform a temperature adjustment in their estimate of HT's LWIR radiative forcing.

Figure 3a shows the 25 km zonal mean MLS water vapor vs latitude. Figure 3b shows the instantaneous tropopause downward LWIR flux change due to the observed H_2O distribution, ΔLWIR. In Fig. 3b-d, the latitude range is restricted because the flux estimates at the poles are very noisy due to tropopause fluctuations. Figure 3c shows ΔSWIR due to the attenuation of water vapor (note the sign change in the color bar). Figure 3d shows the net change in H_2O radiative forcing ΔLWIR+ΔSWIR. The changes in the downward radiative flux follow the evolution of the stratospheric water vapor distribution. There is a small northward shift in aerosols and water vapor shortly after the eruption, and an additional small northward shift of the water vapor distribution in April associated with the QBO (Schoeberl et al., 2023).

The question remains: how much of the LWIR forcing increase is due to H_2O and how much is due to the temperature differences between 2022 and the climatology? To quantify this, we take the 2016-2021 temperature climatology and substitute the 2022 water vapor. We also and take the 2022 temperature field and substitute in the 2016-2021 water vapor climatology. These two experiments help isolate the impact of the HT water vapor from natural temperature fluctuations. We find that about 1/3 of the 2022 LWIR flux increase through April is due to the descending QBO thermal anomaly and 2/3 is due to the stratospheric water vapor increase.

3.2.3 Net radiative forcing changes

Figs. 4 a,b show the time series of the net change in radiative forcing (ΔLWIR + ΔSWIR + ΔA) using the YH clear and all sky parameterizations for ΔA. We also show two latitude cross sections on April 15 (Figs. 4c, 4e) and December 1, 2022 (Figs. 4d, 4e). For both clear and all sky ΔA estimates, the aerosol direct forcing overwhelms the heating from stratospheric water vapor. Fig. 4g shows the hemispheric and global average forcing time series. The total SH radiative forcing peaks in June/July. On the other hand, the much smaller Northern Hemisphere (NH) forcing peaks in April/May after the QBO has spread aerosols and trace gases into the NH (Schoeberl et al., 2023).

The climate impact of the HT eruption plume is difficult to estimate since the aerosol and water vapor forcing decreases by more than half from the peak in mid-April to mid-December (Fig. 4d) so the overall HT forcing is transient. However, we can crudely estimate the tropospheric surface temperature response for a transient event using the analyses of the short-term temperature changes due to stratospheric aerosol loading following the Pinatubo eruption. For Pinatubo, Fujiwara et al. (2020) estimated a tropospheric surface temperature decrease of ~ 0.15°C in the years following the eruption due to an average optical depth of ~0.1 (see their Fig. A3). For our estimate, we only consider the shortwave components; the enhanced LWIR is absorbed in the upper troposphere and will not directly affect the surface temperature (Wang and Huang, 2020; Sellitto, 2022). The SH 2022 clear sky average radiative forcing sans the LWIR component is -0.67 W/m^2. Scaling this forcing to Pinatubo, we roughly estimate that the HT 2022 average SH surface temperature change would be $-0.67\ (0.15°/2.67) = -0.037°C$. Using the YH all sky parameterization, the SH temperature change would be -0.025°C. Note that Fujiwara et al.(2020)'s estimate of the Pinatubo surface temperature response is about five times smaller than earlier estimates found in Crutzen (2006). A thermal response this small would be barely detectable against background meteorological variability. We are also neglecting second order climate responses that could occur, such as changes in cloudiness or lapse rate.

4. Summary and Discussion

The Hunga-Tonga-Hunga Ha'apai (HT) eruption produced increased stratospheric water vapor and aerosols primarily in the Southern Hemisphere. Jenkins et al. (2022) suggested that the increased stratospheric water vapor would warm the climate slightly, but their study neglected the role of volcanic aerosols in reducing the solar flux. We use a radiative transfer model to estimate the changes in downward IR flux due to the MLS observed enhanced water vapor layer, and OMPS-LP data to compute the stratospheric AOD. We parameterize the reduction in solar flux due to HT aerosols using past volcanic events (Table 1). Our results are nearly identical to

Yu and Huang (2023) results for clear skies, non-volcanic conditions. We subsequently use their clear and all sky parameterizations to assess the direct solar forcing. The solar flux reduction by aerosols is larger than the net IR flux increase due to stratospheric water vapor. In other words, the direct solar radiative cooling associated with the HT aerosols overwhelms the enhanced thermal radiation from stratospheric water vapor plume. Our results are in good agreement with net radiative forcing changes estimated by Sellitto et al. (2022) and Zhu et al. (2022). We find that the zonal mean peak change in net radiative forcing occurs in May 2022, but the SH average forcing peaks in June/July as the constituents spread throughout the SH. Using the observed impact on tropospheric temperatures from Pinatubo as a scale, Hunga-Tonga would produce an SH annual average surface temperature change of less than -0.038°C for clear skies and -0.021°C for all skies.

Acknowledgements

This work was supported under NASA grants NNX14AF15G, 80NSSC21K1965 and 80NSSC20K1235

Open Research

The RTM used to estimate H_2O IR cooling rates is from Atmospheric and Environmental Research (RTE+RRTMGP) and can be freely downloaded at http://rtweb.aer.com/rrtm_frame.html.

OMPS-LP data, Taha et al. (2021), is available at https://disc.gsfc.nasa.gov/datasets/OMPS_NPP_LP_L2_AER_DAILY_2/summary , DOI: https://doi.org/10.5067/CX2B9NW6FI27 The algorithm is documented in Taha et al. (2021).

SO_2 historical volcanic eruption data is available at the NASA disc. https://disc.gsfc.nasa.gov/datasets/MSVOLSO2L4_4/summary

Aura MLS Level 2 data, Livesey et al. (2021) JPL D-33509 Rev. C, is available at https://disc.gsfc.nasa.gov/datasets?page=1&keywords=AURA%20MLS

References

Aubry, T.J., Staunton-Sykes, J., Marshall, L.R. *et al.* (2021). Climate change modulates the stratospheric volcanic sulfate aerosol lifecycle and radiative forcing from tropical eruptions. *Nat. Commun.* **12**, 4708. https://doi.org/10.1038/s41467-021-24943-7.

Banerjee, A., Chiodo, G., Previdi, M. *et al.* (2019). Stratospheric water vapor: an important climate feedback. *Clim Dyn* **53**, 1697–1710. https://doi.org/10.1007/s00382-019-04721-4

Bourassa, A. E., Zawada, D. J., Rieger, L. A., Warnock, T. W., Toohey, M., & Degenstein, D. A. (2023). Tomographic retrievals of Hunga Tonga-Hunga Ha'apai volcanic aerosol. Geophysical Research Letters, 50, e2022GL101978, https://doi. org/10.1029/2022GL101978

Carn, S. A., N. A. Krotkov, B. L. Fisher, and C. Li, (2022). Out of the blue: volcanic SO_2 emissions during the 2021-2022 Hunga Tonga – Hunga Ha'apai eruptions, Front. Earth Sci., 13, https://doi.org/10.3389/feart.2022.976962

Carn, S.A., L. Clarisse and A.J. Prata (2016), Multi-decadal satellite measurements of global volcanic degassing, J. Volcanol. Geotherm. Res., 311, 99-134, http://dx.doi.org/10.1016/j.jvolgeores.2016.01.002.

Coy, L., P. Newman, K. Wargan, G. Partyka, S. Strahan, and S. Pawson, (2022). Stratospheric Circulation Changes Associated with the Hunga Tonga-Hunga Ha'apai Eruption, Geophys. Res. Lett., 49, https://www.essoar.org/doi/abs/10.1002/essoar.10512388.1

Crutzen, P. J. (2006). Albedo enhancement by stratospheric sulfur injections: A contribution to resolve a policy dilemma?, Climatic Change, 77, 211–220, https://doi.org/10.1007/s10584-006-9101-y.

Dessler, A.E. and M. D. Zelinka, (2015). *Climate Feedbacks*. Gerald R. North(editor-in-chief), J. Pyle and F. Zhang (editors). Encyclopedia of Atmospheric Sciences, 2nd edition, **2**, pp. 18–25, http://dx.**doi**.org/10.1016/B978-0-12-382225-3.00466-7

Dessler, A.E., M. R. Schoeberl, T. Wang, S. Davis, K. H. Rosenlof, (2013) Stratospheric water vapor feedback, PNAS, www.pnas.org/cgi/doi/10.1073/pnas.1310344110

Jenkins, S., C. Smith, M. Allen, and R. Grainger, (2023). Tonga eruption increases chance of temporary surface temperature anomaly above 1.5 °C, Nature Climate Change, 13, 127-129, https://doi.org/10.1038/s41558-022-01568-2

Forster, P.M.D., and K. P. Shine (1999). Stratospheric water vapour changes as a possible contributor to observed stratospheric cooling. Geophys. Res. Lett., 26, 3309–3312.

Fujiwara, M., Martineau, P., and Wright, J. S. (2020). Surface temperature response to the major volcanic eruptions in multiple reanalysis data sets, Atmos. Chem. Phys., 20, 345–374, https://doi.org/10.5194/acp-20-345-2020.

Hansen, J., et al., (2002). Climate forcings in Goddard Institute for Space Studies SI2000 simulations, J. Geophys. Res., 107(D18), 4347, doi:10.1029/2001JD001143.

Huang, Y., M. Zhang, Y. Xia, Y. Hu and S. Son (2016) Is there stratospheric radiative feedback in global warming simulations? Climate Dynamics, doi: 10.1007/s00382-015-2577-2.

Huang, Y., Wang and H. Huang, (2020) Stratospheric water vapor feedback disclosed by a locking experiment, Geophys. Res. Lett. doi:10.1029/2020GL087987.

Khaykin, S.M., de Laat, A.T.J., Godin-Beekmann, S. et al. (2022) Unexpected self-lofting and dynamical confinement of volcanic plumes: the Raikoke 2019 case." Sci Rep 12, 22409. https://doi.org/10.1038/s41598-022-27021-0, 2022

Kloss, C., Berthet, G., Sellitto, P., Ploeger, F., Taha, G., Tidiga, M., Eremenko, M., Bossolasco, A., Jégou, F., Renard, J.-B., and Legras, B. (2021). Stratospheric aerosol layer perturbation caused by the 2019 Raikoke and Ulawun eruptions and their radiative forcing, Atmos. Chem. Phys., 21, 535–560, https://doi.org/10.5194/acp-21-535-2021

Li, F., P. Newman (2020) Stratospheric water vapor feedback and its climate impacts in the coupled atmosphere–ocean Goddard Earth Observing System Chemistry-Climate Model. *Clim Dyn* **55**, 1585–1595 https://doi.org/10.1007/s00382-020-05348-6

Livesey, N., Read, W.G., Wagner, P.A., Froidevaux, L., Santee, M.L., Schwartz, M.J. et al. (2021). Earth Observing System (EOS) Aura Microwave Limb Sounder (MLS) version 5.0x level 2 and 3 data quality and description document, JPL D-105336 Rev A. https://mls.jpl.nasa.gov/data/v5-0_data_quality_document.pdf

Millán, L. et al., (2022). The Hunga Tonga-Hunga Ha'apai Hydration of the Stratosphere, Geophysical Research Letters. 49, e2002GL099381,https://doi.org/10.1029/2022GL099381

Mlawer, E.J., S.J. Taubman, P.D. Brown, M.J. Iacono and S.A. Clough (1997). RRTM, a validated correlated-k model for the longwave. *J. Geophys. Res.*, **102**, 16,663-16,682.

Pitari, G., G. Di Genova, E. Mancini, D. Visioni, I Gandolfi, and I. Cionni, (2016) Stratospheric Aerosols from Major Volcanic Eruptions: A Composition-Climate Model Study of the Aerosol Cloud Dispersal and e-folding Time, Atmosphere, 7, doi:10.3390/atmos7060075.

Schoeberl, M. R., Wang, Y., Ueyama, R., Taha, G., Jensen, E., & Yu, W. (2022). Analysis and impact of the Hunga Tonga-Hunga Ha'apai stratospheric water vapor plume. Geophysical Research Letters, 49, e2022GL100248. https://doi.org/10.1029/2022GL100248

Schoeberl, M. R., Wang, Y., Ueyama, R., Taha, G.,& Yu, W. (2023).

The Cross Equatorial Transport of the Hunga Tonga-Hunga Ha'apai Eruption Plume. Geophysical Research Letters, 49, e2022GL10443, https://doi.org/10.1029/2022GL102443

Sellitto, P., R Siddans, R. Belhadji, E. Carboni, B.Legras, A. Podglajen, C. Duchamp, and B. Kerridge (2023), Observing the SO2 and Sulphate Aerosol Plumes from the 2022 Hunga Tonga-Hunga Ha'apai Eruption with IASI, https://doi.org/10.1038/s43247-022-00618-z

Sellitto, P., R. Belhadji, M. Boichu, E. Carboni, J. Cuesta, C. Duchanp, C. Kloss, R. Siddans, N. Begue, L. Blarel, F. Jegou, S. Khaykin, H-B. Renard, and B. Legras, (2023) https://doi.org/10.22541/essoar.169091894.48592907/v1

Solomon, S., Rosenlof, R. Portmann, J. S. Daniel, S. M. Davis, T. J. Sanford, G-K. Plattner, (2010). Contributions of Stratospheric Water Vapor to Decadal Changes in the Rate of Global Warming, Science, 237, 1219-1221, doi:10.1126/science.1182488

Stenchikov, G. (2016). The Role of Volcanic Activity in Climate and Global Change, 2nd Edn., Elsevier, Boston, Massachusetts, USA, https://doi.org/10.1016/B978-0-444-63524-2.00026-9 .

Taha, G., R. Loughman, T. Zhu, L. Thomason, J. Kar, L. Rieger, and A. Bourassa (2021). OMPS LP Version 2.0 multi-wavelength aerosol extinction coefficient retrieval algorithm, Atmos. Meas. Tech., 14, 1015–1036, https://doi.org/10.5194/amt-14-1015-2021.

Taha, G., R. Loughman, P. Colarco, T. Zhu, L. Thomason, G. Jaross (2022). Tracking the 2022 Hunga Tonga-Hunga Ha'apai aerosol cloud in the upper and middle stratosphere using space-based observations, Geophy. Res. Lett., https://doi.org/10.1029/2022GL100091..

Vömel, H., S. Evan, and M. Tully (2022). Water vapor injection into the stratosphere by Hunga Tonga-Hunga Ha'apai, Science, 377,1444-1447.

Wang, Y., & Huang, Y. (2020). The surface warming attributable to stratospheric water vapor in CO2-caused global warming. J. of Geophys. Res.: Atmospheres, 125, e2020JD032752. https://doi.org/10.1029/2020JD032752

Xia, Y., Y. Huang, Y. Hu, and J. Wang (2019). Impacts of tropical tropopause warming on the stratospheric water vapor. *Clim. Dyn.*, **53**, 3409–3418. https://doi.org/10.1007/s00382-019-04714-3

Yu, Q., & Huang, Y. (2023). Distributions and trends of the aerosol direct radiative effect in the 21st century: Aerosol and environmental contributions. Journal of Geophysical Research: Atmospheres, 128, e2022JD037716. https://doi.org/10.1029/2022JD037716

Zhu et al., (2022). Perturbations in stratospheric aerosol evolution due to the water-rich plume of the 2022 Hunga-Tonga eruption, Communications Earth & Environment, 3, 248, https://doi.org/10.1038/s43247-022-00580-w

Table 1. Estimated emission SO_2, the maximum globally averaged AOD (550 nm) and decrease in global solar flux for indicated large volcanic events. We also show the change in direct forcing (1) and the YH parameterization. We use the Raikoke AOD maps shown in Kloss et al. (2020) to estimate the Raikoke AOD. SO_2 amounts used by the authors shown; amounts in parenthesis are from the NASA database, Carn et al.(2022), and Sellitto et al. (2023) for HT.

Eruption	Date	SO_2 (Tg)	Max AOD	ΔA W/m^2	$\log_e$ fit ΔA W/m^2	YH ΔA W/m^2 clear/cloudy	Reference
Agung	May, 1963	12	0.11	-2.9	-2.8	-3.2/-1.7	Pitari et al. (2016)
El Chichón	April, 1982	7 (8)	0.05	-1.75	-1.8	-1.4/-0.78	Pitari et al. (2016)
Nevado del Ruiz	Nov., 1985	1.2 (0.7)	0.015	-0.3	-0.29	-0.44/-0.23	Pitari et al. (2016)
Pinatubo	June, 1991	20 (17)	0.2	-3.5	-3.55	-5.88/-3.14	Pitari et al. (2016)
Raikoke	June, 2019	(1.4)	0.016	-0.4	-0.41	-0.48/-0.26	Kloss et al. (2020)
LE Sim.	-	10	0.15	-3.2	-3.2	-4.4/-2.3	Aubry et al. (2021)
Hunga-Tonga	Jan., 2022	(0.5-1.5)	0.018		-0.64	-0.59/-0.31	This paper

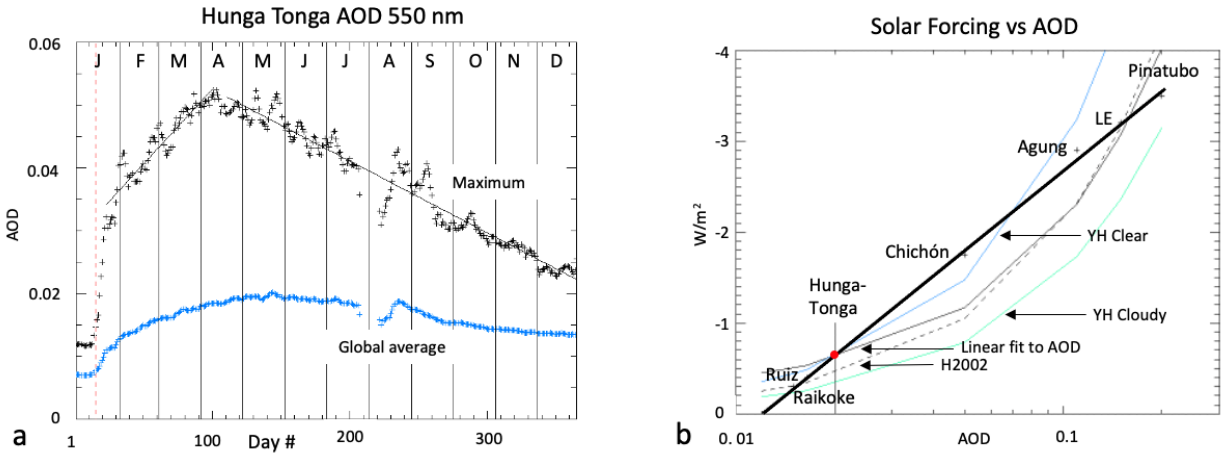

Figure 1. Part a, OMPS-LP measured AOD vs time following the HT eruption. Crosses are the maximum AOD, blue crosses are the global average. A spacecraft anomaly resulted in missing measurements from late July to mid-August. Black lines show linear fits to the data. Part b, changes in solar forcing with AOD for volcanic eruptions shown in Table 1. The $\log_e$ fit (1) is the thick solid line. Linear fits from H2002 and the Table 1 data are shown as dashed and thin solid lines. The YH clear and cloudy fits are shown in blue and green lines. Volcanic events are small crosses next to the names. The red dot indicates HT (Part a, blue curve).

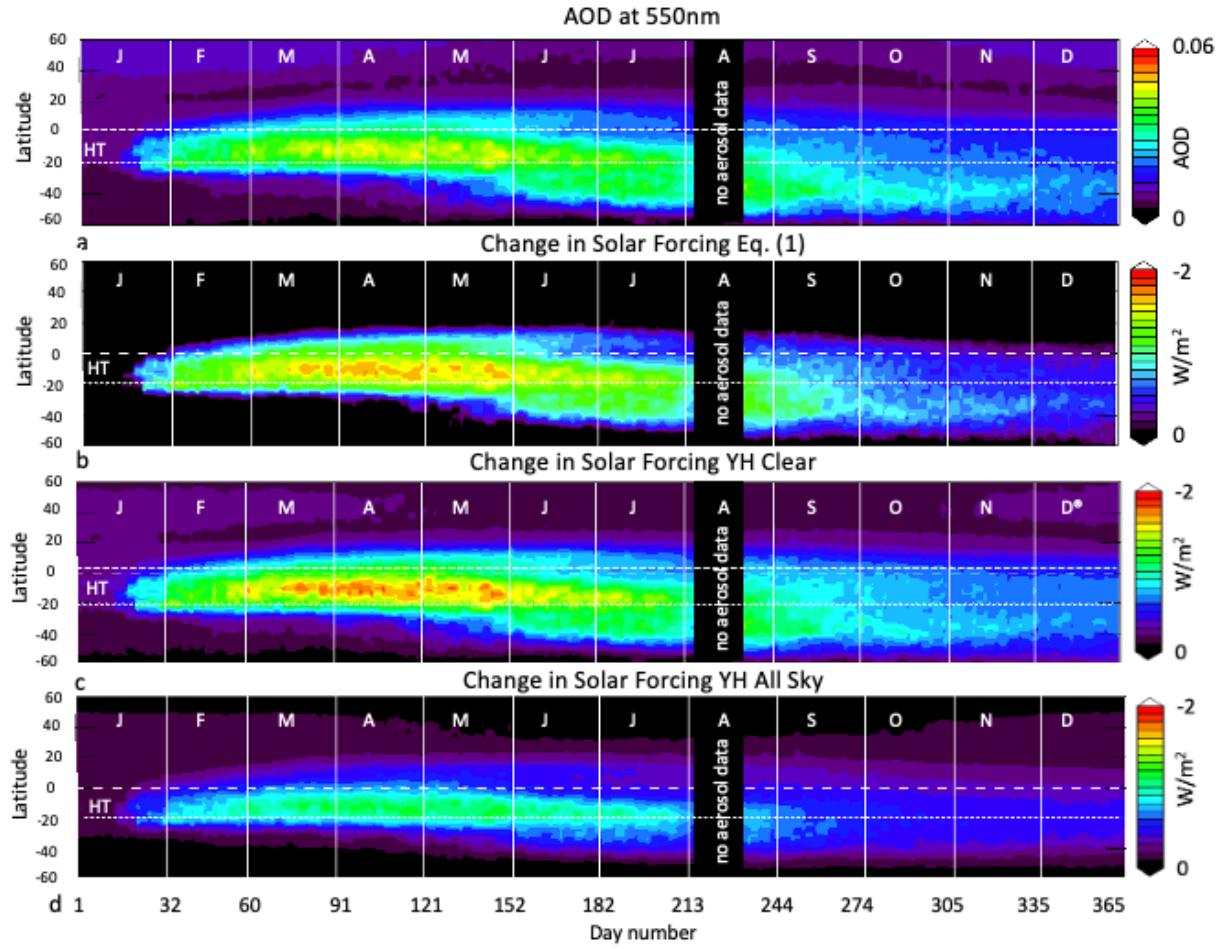

Figure 2 Part a, changes in stratospheric OMPS-LP AOD vs time during 2022. Part b, change in solar forcing due to AOD using Eq. (1). Part (c, d) shows the forcing using the YH kernels for clear sky and all skies. Vertical lines divide months with initial shown, dotted line is the latitude of HT, dashed line locates the equator.

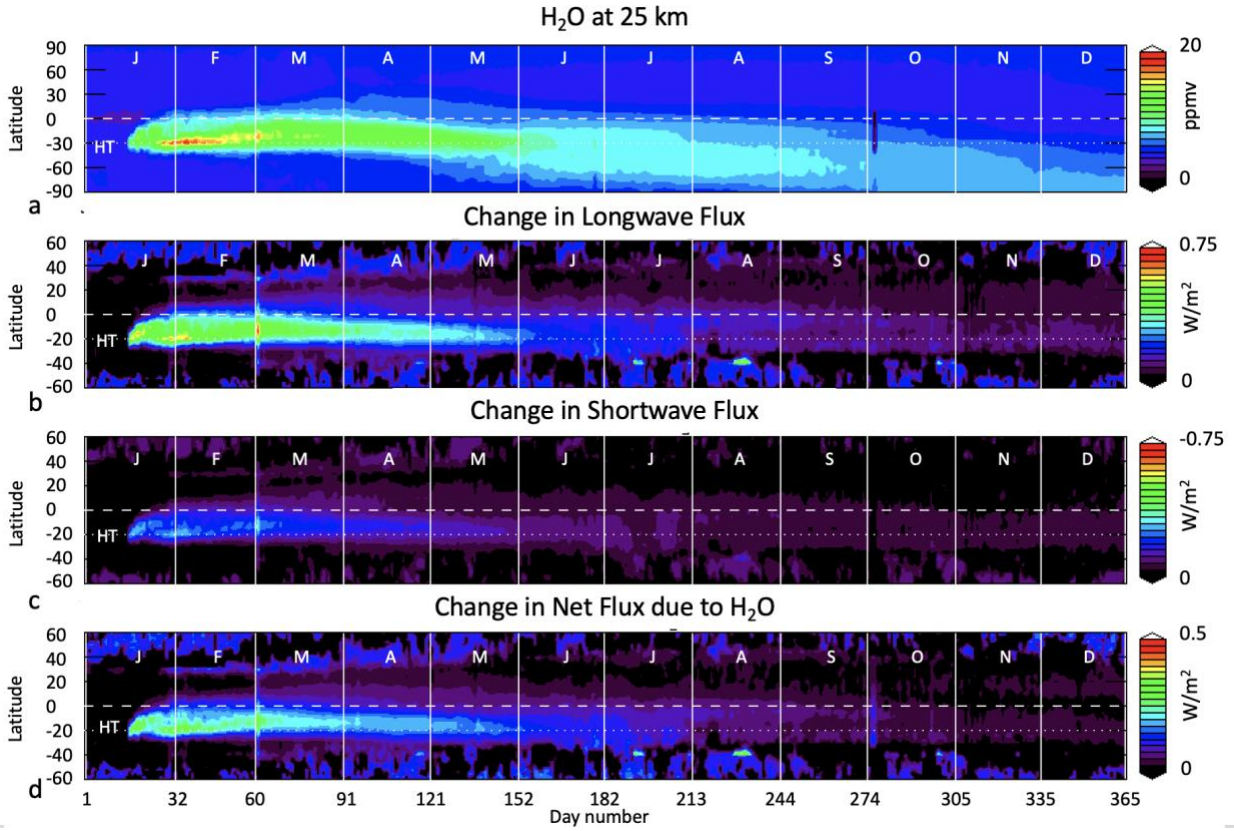

Figure 3 Part a, 2022 zonal mean water vapor at 25 km. Part b, change in LWIR downward flux at the tropopause. Part c, change in SWIR downward flux at the tropopause. Note the sign change in the color bar. Part d, net flux change.

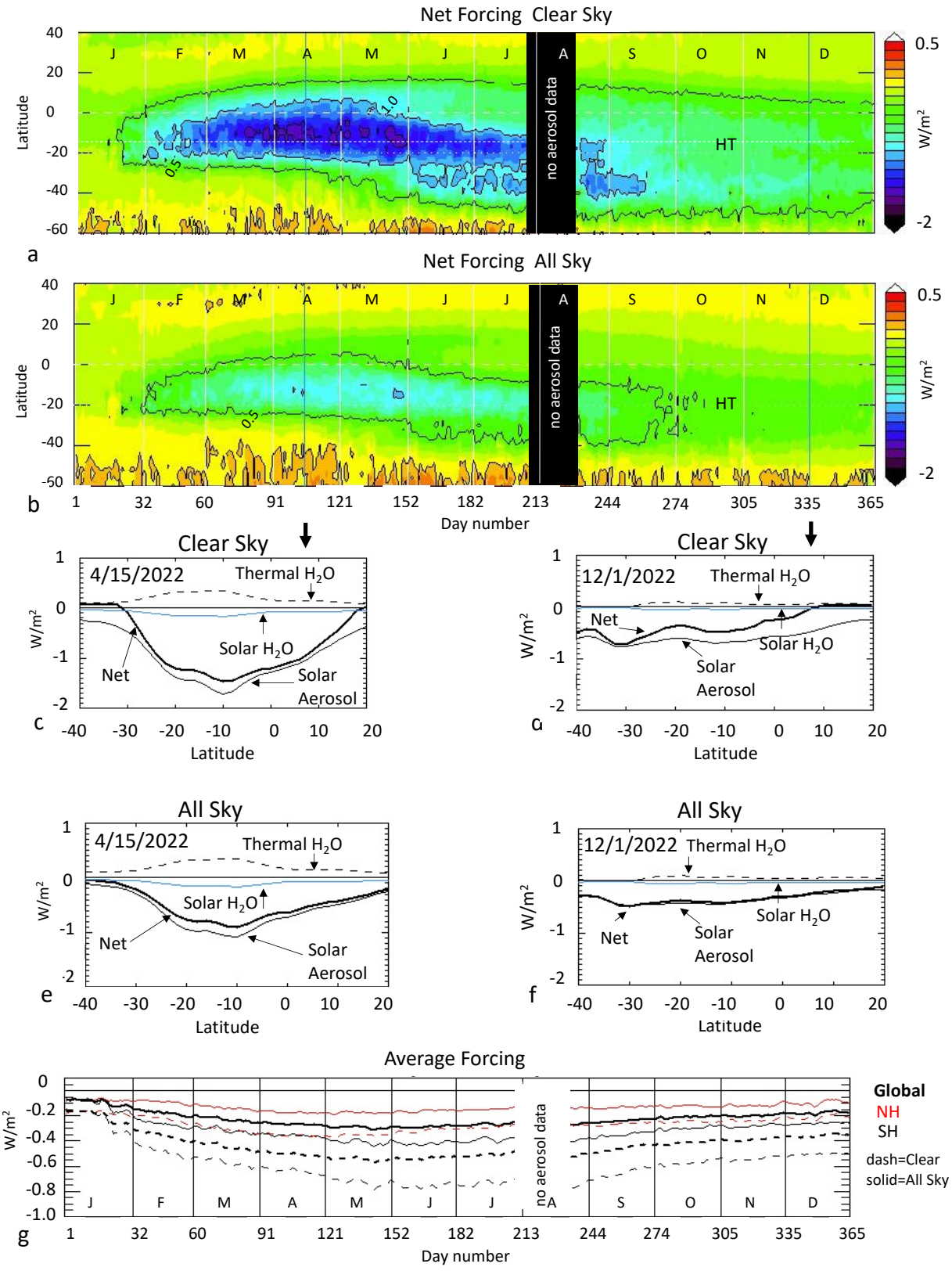

Figure 4 Part a, net radiative forcing using YH clear sky solar forcing (Fig. 2c) and IR forcing change (Fig. 3d). Part b, same as part a using YH all sky solar forcing. Parts c, e show the

components of the forcing vs latitude on 4/15/2022 and parts d, f for 12/1/2022, clear and all sky forcing. Part g shows hemispheric average and global average forcing, thick black line is global, red line is NH and thin line is SH; dashed lines for clear, and solid for all sky.